The Plant Cell, Vol. 29: 1642–1656, July 2017, www.plantcell.org © 2017 ASPB.



# ZHOUPI and KERBEROS Mediate Embryo/Endosperm Separation by Promoting the Formation of an Extracuticular Sheath at the Embryo Surface

**Steven Moussu,[a] Nicolas M. Doll,[a] Sophy Chamot,[a] Lysiane Brocard,[b,c,d] Audrey Creff,[a] Chloé Fourquin,[a] Thomas Widiez,[a] Zachary L. Nimchuk,[e,f] and Gwyneth Ingram[a,1]**

[a] Laboratoire Reproduction et Développement des Plantes, Université de Lyon, ENS de Lyon, UCB Lyon 1, CNRS, INRA, F-69342 Lyon, France
[b] Centre National de la Recherche Scientifique/University of Bordeaux, Plant Imaging Platform of Bordeaux Imaging Center, UMS 3420, F-33000 Bordeaux, France
[c] Université de Bordeaux, Laboratoire de Biogenèse Membranaire, UMR5200, F-33000 Bordeaux, France
[d] Centre National de la Recherche Scientifique, Laboratoire de Biogenèse Membranaire, UMR5200, F-33000 Bordeaux, France
[e] Department of Biology, University of North Carolina at Chapel Hill, Chapel Hill, North Carolina 27599-3280
[f] Curriculum in Genetics and Molecular Biology, University of North Carolina at Chapel Hill, Chapel Hill, North Carolina 27599-3280

ORCID IDs: 0000-0002-9397-1660 (L.B.); 0000-0001-6002-2306 (T.W.); 0000-0002-1425-9545 (G.I.)

***Arabidopsis thaliana*** **seed development requires the concomitant development of two zygotic compartments, the embryo and the endosperm. Following fertilization, the endosperm expands and the embryo grows invasively through the endosperm, which breaks down. Here, we describe a structure we refer to as the embryo sheath that forms on the surface of the embryo as it starts to elongate. The sheath is deposited outside the embryonic cuticle and incorporates endosperm-derived material rich in extensin-like molecules. Sheath production is dependent upon the activity of ZHOUPI, an endosperm-specific transcription factor necessary for endosperm degradation, embryo growth, embryo-endosperm separation, and normal embryo cuticle formation. We show that the peptide KERBEROS, whose expression is ZHOUPI dependent, is necessary both for the formation of a normal embryo sheath and for embryo-endosperm separation. Finally, we show that the receptor-like kinases GSO1 and GSO2 are required for sheath deposition at the embryo surface but not for production of sheath material in the endosperm. We present a model in which sheath formation depends on the coordinated production of material in the endosperm and signaling within the embryo, highlighting the complex molecular interaction between these two tissues during early seed development.**

## INTRODUCTION

Angiosperm seed development is a complex process requiring the coordinated development of three structurally and genetically distinct compartments: the maternal seed coat and the zygotic endosperm and embryo. These three tissues are arranged one inside the other and must communicate both chemically and physically during seed growth to coordinate their development (Ingram, 2010). The endosperm surrounds the developing embryo and plays two critical roles in seed development. The first is to grow and to generate space within the maternal seed coat for nutrient storage, and the second is to act as a sink tissue, absorbing nutrients from the mother plants and transferring them to the developing embryo during seed development and germination (Berger, 2003; Li and Berger, 2012; Olsen, 2004).

In *Arabidopsis thaliana*, the endosperm is a largely transient compartment, which grows rapidly as a multinucleate coenocyte after fertilization, cellularizes, and then degenerates as it is replaced by the expanding embryo. The interaction between the embryo and the endosperm during this stage of development is relatively poorly understood, but involves the physical invasion of, the endosperm by the embryo. This type of interaction between two plant tissues is relatively rare during normal development. A similar example is the movement of the pollen tube through the tissues of the style during fertilization (Cheung et al., 2010). Interestingly, both of these interactions involve the movement of one tissue through a genetically distinct neighboring tissue.

The endosperm-specific bHLH transcription factor ZHOUPI/RETARDED GROWTH OF EMBRYO1 (ZOU/RGE1) (Kondou et al., 2008; Yang et al., 2008) acts as a heterodimer with a second bHLH called ICE1 (Denay et al., 2014) and has been shown to regulate the embryo/endosperm interaction in Arabidopsis. To date, ZOU has been shown to be required for two partially separable processes. The first is endosperm breakdown. ZOU regulates the expression of a range of cell wall-modifying enzymes in the endosperm, and endosperm cell wall softening by these enzymes appears to be necessary to permit crushing of the endosperm during embryo expansion (Fourquin et al., 2016). As a result, the mature seeds of *zou* mutants contain a large body of persistent endosperm in addition to the specialized outer endosperm cell layer, which is all that remains in mature wild-type seeds. A second function of the ZOU/ICE1 complex is to participate in the formation of an intact

[1] Address correspondence to gwyneth.ingram@ens-lyon.fr.
The author responsible for distribution of materials integral to the findings presented in this article in accordance with the policy described in the Instructions for Authors (www.plantcell.org) is: Gwyneth Ingram (gwyneth.ingram@ens-lyon.fr).
www.plantcell.org/cgi/doi/10.1105/tpc.17.00016

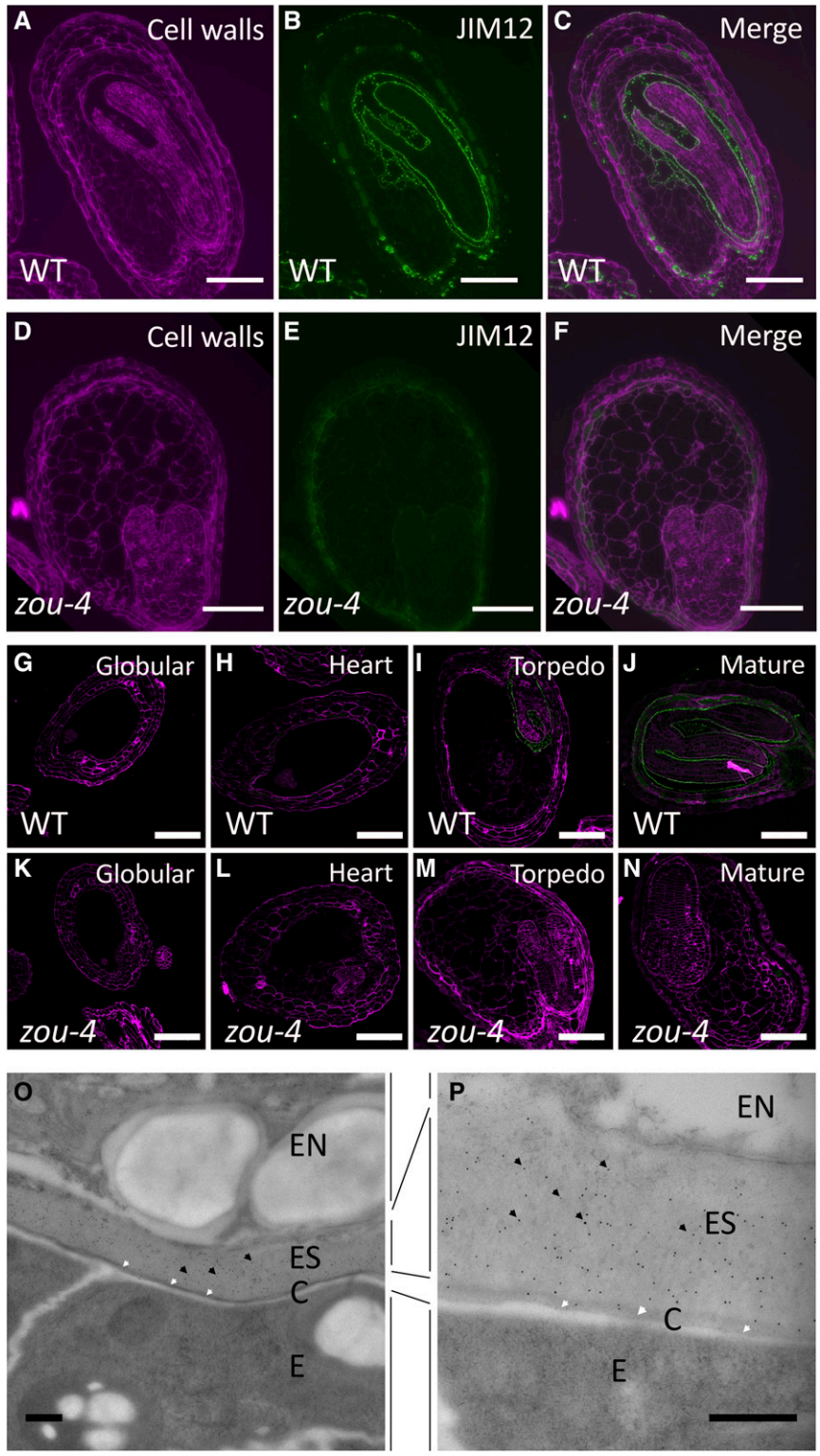


**Figure 1.** An Extracuticular Sheath-Like Structure Surrounds the Developing Arabidopsis Embryo, and Its Formation Is ZOU Dependent.

**(A)** to **(N)** Fluorescent immunolabeling with the α-JIM12 antibody. Photographs are of torpedo stage wild-type Col-0 seed (**[A]** to **[C]**) and torpedo stage *zou-4* seed (**[D]** to **[F]**) showing calcofluor staining of cell walls (**[A]** and **[D]**), the α-JIM12 signal (**[B]** and **[E]**), and merged images (**[C]** and **[F]**).

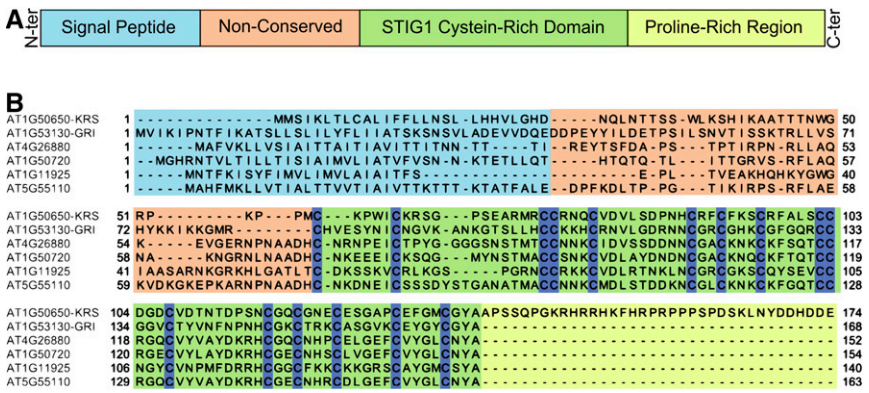


**Figure 2.** KRS Is a Unique Member of a Small Protein Family.

**(A)** Subdivision of the KRS amino acid sequence into different domains based on alignment data.
**(B)** Alignment of the KRS sequence with sequences of the other STIG1-like Arabidopsis proteins. The conserved cysteine residues in the STIG1 domain are highlighted in dark blue.

embryonic cuticle. This function appears to be achieved, at least in part, through the regulation of the expression of ALE1, a subtilisin serine protease that acts in an intercompartment signaling pathway involving the receptor-like kinases GSO1 and GSO2 (Tanaka et al., 2001; Tsuwamoto et al., 2008; Xing et al., 2013). Like *ale1* mutant embryos, *zou* mutant embryos produce a discontinuous cuticle on the surface of the developing embryo (Tanaka et al., 2001; Yang et al., 2008).

In addition to the two phenotypes described above, *zou* mutants show strong adhesion of the embryonic surface to surrounding endosperm cells. During plant development, normal cuticle formation is generally considered to play an important role in preventing the fusion of developing organs with their neighbors (Delude et al., 2016). Therefore, the embryo/endosperm adhesion phenotype of *zou*, *ale1*, and *gso1/gso2* mutants has been attributed to defects in the embryonic cuticle. But although the cuticle of *zou* mutant embryos is defective, it is present over most of the embryonic surface. Interestingly, an abnormal deposition of endosperm debris on apparently intact zones of cuticle has been reported in *zou* mutant seedlings (Xing et al., 2013), suggesting that embryo/endosperm adhesion defects may not be solely due to cuticle discontinuities.

Here, we show that ZOU is required for the production of an extracuticular endosperm-derived structure—which we have named the embryo sheath—at the surface of the embryo. We show that ZOU is required for production of KERBEROS, a unique, endosperm-specific cysteine-rich peptide that is necessary for the biogenesis of the embryo sheath, for embryo-endosperm separation, and for normal progression of the embryo through the endosperm tissue. We propose that the embryo sheath provides a separation/lubrication function facilitating the movement of the embryo relative to the degenerating endosperm and provide a model describing the molecular interactions between the embryo/endosperm required for sheath biogenesis.

## RESULTS

### The Deposition of a Sheath Covering the Developing Embryo Is Absent in *zou* Mutants

Previous studies have shown that the surface of the mature embryo of Arabidopsis is covered with a continuous structure that is detected by the antiextensin antibodies α-JIM12 (Smallwood et al., 1994) and α-LM1 (Lee et al., 2012; Smallwood et al., 1995). We analyzed the deposition of this structure during embryogenesis in seeds of wild-type plants and *zou* mutant plants. We first detected deposition of this structure at the late heart stage of embryo development, when embryo separation from the endosperm first becomes apparent, in a thin layer covering the embryo surface (Figures 1A to 1C and 1G to 1J). In addition, we observed labeling of vesicle-like structures in some of the endosperm cells immediately adjacent to the embryo Figures 1A to 1C and Supplemental Figure 1. A similar pattern was detected throughout the rest of embryo development, with labeling detected at the embryo surface and in the adjacent endosperm, but never in the developing embryo (Figures 1G to 1J; Supplemental Figure 1). During chemical fixation for immunolocalizations, the endosperm retracts from the embryo, possibly due to tissue shrinkage during dehydration, highlighting the separation of these two organs. A reticulate pattern of labeling was also observed in the large extracellular space resulting from this retraction of the endosperm from the embryo. This labeling pattern strongly suggests that the

**Figure 1.** (continued).

**(G)** to **(N)** Developmental time course of embryo sheath deposition in wild-type Col-0 (**[G]** to **[J]**) and in *zou-4* (**[K]** to **[N]**). Stages from globular to mature embryo are indicated. Bar = 100 μm.
**(O)** and **(P)** Transmission electron microscopy images of immunogold labeling of torpedo stage wild-type Col-0 seeds at the embryo-endosperm interface using the α-JIM12 antibody. Bar = 100 nm. The different seed compartments are indicated between parts **(O)** and **(P)**. Gold particles are visible as black spots and some are indicated by black arrows. C, cuticle; E, embryo; EN, endosperm; ES, embryo sheath.

material making up the α-LM1/α-JIM12 labeled sheath is produced by the endosperm and deposited at the interface between the endosperm and the embryo as it develops.

When immunolocalizations were performed under identical conditions in a *zou-4* mutant background, we were unable to detect labeling with α-LM1 or α-JIM12 in either the endosperm or at the embryo surface at any time during seed development (Figures 1D, 1E, and 1K to 1N; Supplemental Figure 1). This suggests that the production of the sheath depends upon ZOU function. Furthermore, as previously described, we observed no separation between the embryo and the endosperm in *zou-4* mutants.

To determine more clearly the relative positions of the embryonic cuticle and the material within the embryonic sheath, we performed immunogold labeling experiments using wild-type embryos at the early torpedo stage. Seeds were fixed using a freeze-substitution protocol and retraction of the endosperm from the developing embryo was not observed. This experiment revealed that the α-JIM12 and α-LM1 antibodies react strongly with an electron-translucent layer of material that is located between the embryonic cuticle and the endosperm (Figures 1O and 1P; Supplemental Figure 2). This supports the immunofluorescence data, suggesting that this structure originates from the endosperm.

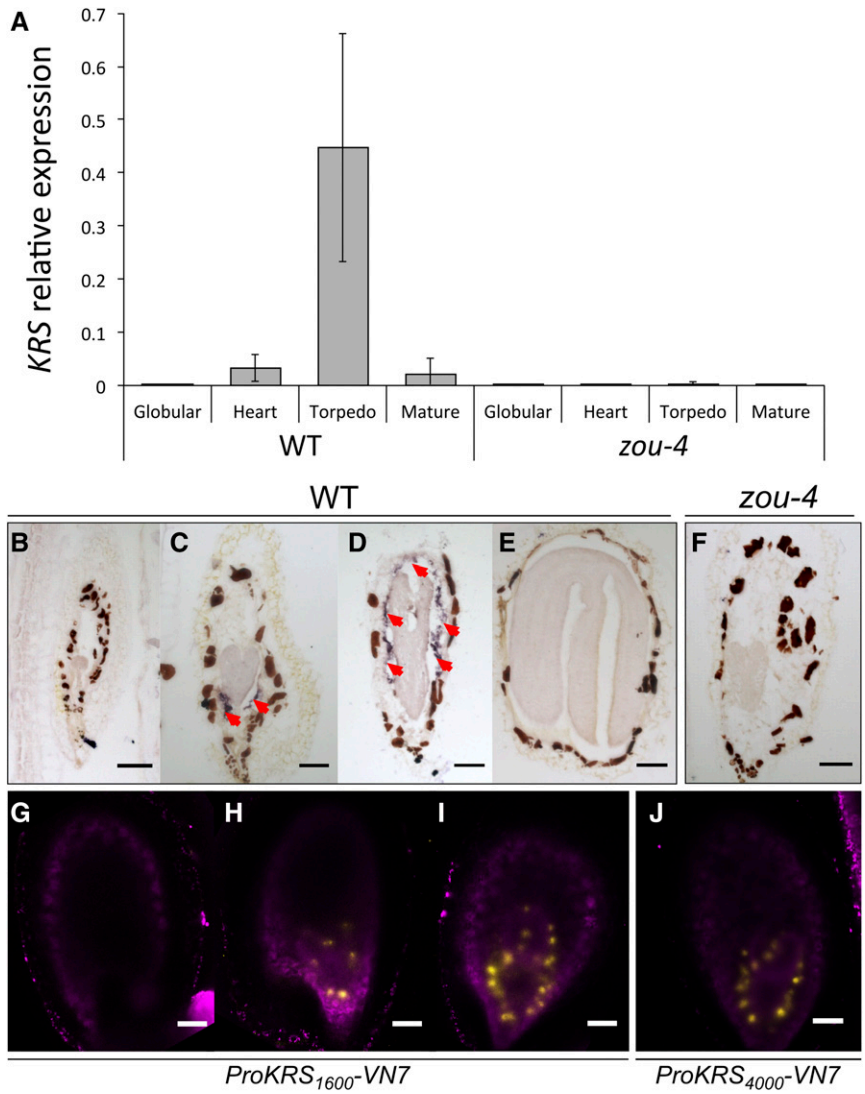


**Figure 3.** *KRS* Expression Is Restricted to the Endosperm in Seeds and Is ZOU Dependent.

**(A)** Expression of *KRS* relative to that of *EIF4* in the wild-type and *zou-4* siliques; error bars represent standard errors. Three biological replicates were used.
**(B)** to **(F)** In situ hybridization using *KRS* antisense probe. Photographs show wild-type Col-0 (**[B]** to **[E]**) and *zou-4* mutant **(F)**. Globular **(B)**, heart **(C)**, torpedo (**[D]** and **[F]**), and mature **(E)**. True signal is blue/black in color and is indicated with red arrows. The brown coloration of the endothelium (inner cell layer of the seed coat) is observed in all seeds and is an accepted artifact in developing seed tissues. Bars = 100 μm.
**(G)** to **(J)** Confocal imaging of *ProKRS*$_{1600}$*-VN7* and *ProKRS*$_{4000}$*-VN7* harboring seeds. VENUS fluorescence is shown in yellow and autofluorescence in magenta. Developmental stages: globular **(G)**, late heart **(H)**, and torpedo (**[I]** and **[J]**). Bars = 100 μm

### ZOU Activity Is Necessary for the Expression of KERBEROS, a Cysteine-Rich Peptide with a C-Terminal Proline-Rich Domain

Extensins are a class of hydroxyproline-rich glycoproteins found in plant cell walls (Lamport, 1973; Liu et al., 2016; Tierney and Varner, 1987). Transcriptional analysis of *zou-4* mutant seeds compared with wild-type seeds (Xing et al., 2013) revealed a number of potential ZOU-regulated genes encoding predicted proline-rich secreted peptides. The most strongly downregulated gene in this class, *AT1G50650*, encodes a cysteine-rich peptide of the STIG1 family. We named this peptide KERBEROS (KRS) after the mythical guardian of the underworld who separates the dead from the living. STIG1-like peptides are named after the founding member of this protein family, STIGMA-SPECIFIC PROTEIN1, which regulates the production of a stigma exudate in tobacco (*Nicotiana tabacum*), petunia (*Petunia hybrida*), and tomato (*Solanum lycopersicum*) (Huang et al., 2014; Tang et al., 2004; Verhoeven et al., 2005). Based on sequence homologies with the other five members of the STIG1 family in Arabidopsis, we defined four different domains in KRS (Figure 2A): (1) a signal peptide predicted to be necessary for targeting to the secretory pathway,

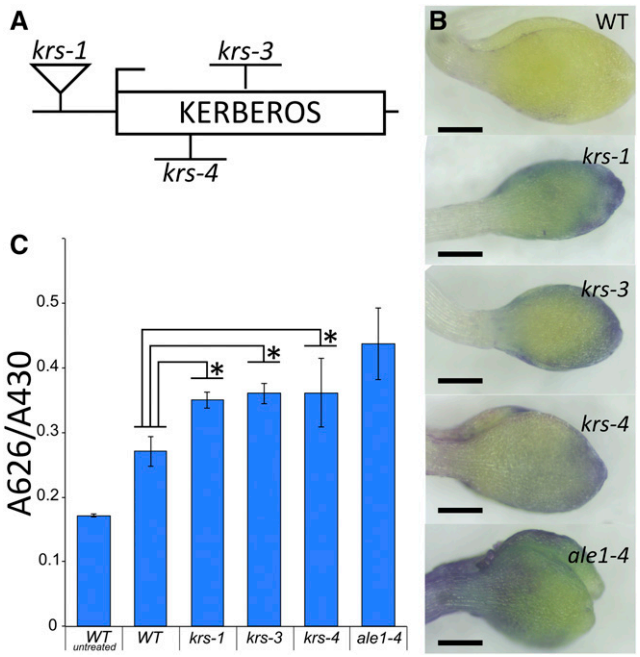


**Figure 4.** Loss of KRS Function Leads to Increased Embryonic Cuticle Permeability.

**(A)** Schematic representation of *KRS* showing the location of mutations in the *krs* alleles used during this study (details of CRISPR alleles are shown in Supplemental Figure 7).
**(B)** Evaluation of toluidine blue permeability in etiolated seedlings from *krs* mutant backgrounds. Wild-type Col-0 was used as a negative control and *ale1-4* as a positive control. Bar = 100 μm.
**(C)** Toluidine blue permeability quantification in the wild type and the *krs* mutants. Error bars represent SD from three biological replicates. Black stars indicate statistically significant differences ($P < 0.01$) obtained after ANOVA and subsequent Tukey HSD tests.

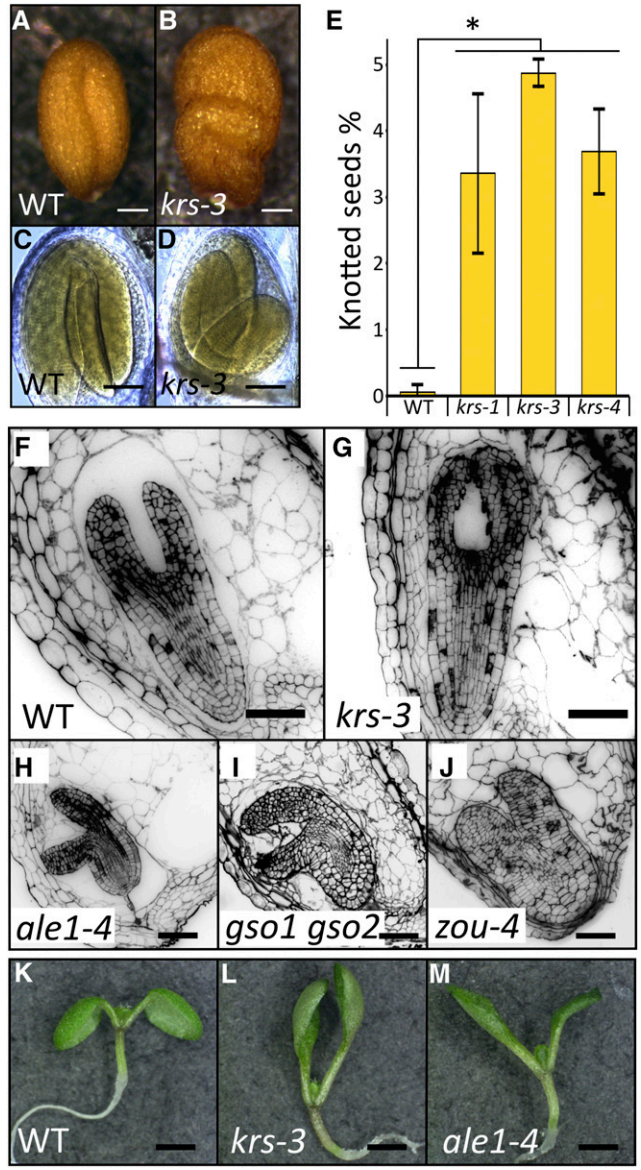


**Figure 5.** Loss of KRS Function Causes Seed Shape Defects and Adhesion of the Endosperm to the Embryo Surface.

**(A)** and **(B)** Mature seeds of wild-type Col-0 **(A)** and knotted *krs-3* **(B)**. Bar = 100 μm
**(C)** and **(D)** Cleared developing seeds showing equivalent phenotypes Col-0 seed **(C)** and *krs-3* knotted seed **(D)**. Bar = 100 μm.
**(E)** Penetrance of the seed shape phenotype: percentage of misshapen seeds observed in the different *krs* mutant alleles analyzed in this study and in wild-type plants. Three biological replicates were used for each genotype. Error bars represent standard deviations. Asterisk indicates statistically significant differences ($P < 0.01$) obtained after ANOVA and subsequent Tukey HSD tests.
**(F)** to **(J)** Endosperm/embryo adhesion visualized in thin sections stained with calcofluor. Col-0 **(F)**, *krs-3* **(G)**, *ale1-4* **(H)**, *gso1 gso2* **(I)**, and *zou-4* **(J)**. Bars = 50 μm.
**(K)** to **(M)** Seedling cotyledon cupping phenotype. Col-0 **(K)**, *krs-3* **(L)**, and *ale1-4* **(M)**. Bars = 2 mm.

(2) a nonconserved region with very low similarity to the other family members from Arabidopsis, (3) the cysteine-rich STIG1 domain, and (4) a domain unique to KRS that contains a stretch of basic residues followed by a sequence that is proline rich (and thus potentially glycosylated) but lacks known extensin motifs (Figure 2B).

To examine the evolutionary relevance of the KRS-specific proline-rich region, we performed a phylogenetic analysis on all the STIG1-like peptides from representative sequenced genomes (https://phytozome.jgi.doe.gov/pz/portal.html). Basing the phylogenetic analysis on alignments of the conserved STIG1 domain, the KRS-like peptides (defined by the presence of the C-terminal proline-rich sequence) fall into a distinct clade that is separate from other STIG1-like proteins found in Arabidopsis and other species (Supplemental Figure 3). Proteins from this clade appear to be present in most eudicots, but no KRS-like STIG1-like peptides have been found in monocots. Alignment of the KRS-specific C-terminal domain from KRS-like peptides of a variety of other eudicots does not reveal any highly conserved motifs. However, this domain almost always contains an array of several proline residues and SP motifs, which are often targets of proline hydroxylation, possibly indicating the presence of hydroxyproline substitutions in the mature form of the peptides (Shi et al., 2015).

We investigated the spatial and temporal patterns of *KRS* expression by detecting *KRS* mRNA and by promoter activity studies. Public microarray data (http://bar.utoronto.ca/efp/cgi-bin/efpWeb.cgi) (Le et al., 2010; Winter et al., 2007) indicates primarily seed-specific expression for *KRS*, with strong specificity for the endosperm (Supplemental Figure 4). RT-qPCR and in situ hybridizations with *KRS* mRNA transcripts confirmed this expression pattern. Temporally, *KRS* expression begins at the heart stage, increases during embryo growth, and decreases as the embryo reaches its final size (Figure 3A). Spatially, *KRS* expression is restricted to the endosperm cells immediately surrounding the embryo (Figures 3B to 3D).

We studied *KRS* promoter activity using either the 1600-bp ($ProKRS_{1600}$) or the 4000-bp ($ProKRS_{4000}$) sequences upstream of *KRS* to drive the expression of YFP (VENUS) carrying a N7 nuclear localization tag (referred to as VN7). In seeds, VN7 accumulation in transgenic plants was endosperm specific for both $pKRS_{1600}$-*VN7* (Figures 3G to 3I) and $ProKRS_{4000}$-*VN7* (Figure 3J), suggesting that the 1600-bp upstream sequence is sufficient to drive *KRS* expression. The signal was first observed around the base of the embryo at the heart stage and then surrounding the embryo during its growth (Figures 3G to 3I).

Weak expression was also observed in some root cell types using in silico data (Brady et al., 2007). Consistent with these in silico data, we also observed weak expression of the *KRS* promoter in an internal cell layer of the expanding root (Supplemental Figure 5).

Because regulation of *KRS* expression by ZOU had previously been suggested by RNA-seq experiments (Xing et al., 2013), we investigated *KRS* expression in *zou-4* mutants (Yang et al., 2008). Using RT-qPCR, we could not detect *KRS* transcripts in *zou-4* mutants during seed development (Figure 3A). Consistent with this result, in situ hybridizations using a *KRS* antisense probe detected no transcripts in torpedo stage *zou-4* seeds (Figure 3F). Taken together, these results show that *KRS* expression in seeds is restricted to the endosperm immediately surrounding the embryo, beginning at the heart stage and peaking at the torpedo stage before disappearing as the endosperm is lysed. Our data also demonstrate that *KRS* expression is dependent upon ZOU activity. However, the fact that *KRS* expression is also observed in roots, together with the relatively late onset of *KRS* expression, suggests that *KRS* is probably not a direct target of the ZOU/ICE1 transcription factor complex.

## KRS Is Required for Normal Embryo Growth and Embryonic Cuticle Integrity

To investigate *KRS* function in the seed, we generated a series of knockdown and knockout mutants. A publicly available insertion line with a T-DNA insertion in the *KRS* promoter (GABI_824G07; Figure 4A) was found to have residual expression of *KRS* in the seed (Supplemental Figure 6). We named this knockdown allele *krs-1*. A second available T-DNA allele with a nearly identical insertion site was present in mutant collections and we named this *krs-2*. This allele was not characterized in our study. To generate independent knockout alleles of *KRS*, we used CRISPR/Cas9 technology to target the *KRS* genomic sequence (Peterson et al., 2016; Schiml et al., 2016). We obtained two independent alleles that each contain insertions of 1 bp, causing a frame shift, and we named them *krs-3* and *krs-4* (Figure 4A; Supplemental Figure 7).

We performed both qualitative and quantitative toluidine blue permeability assays on cotyledons to test for cuticle integrity in mutants and overexpression lines (Xing et al., 2013; Denay et al.,

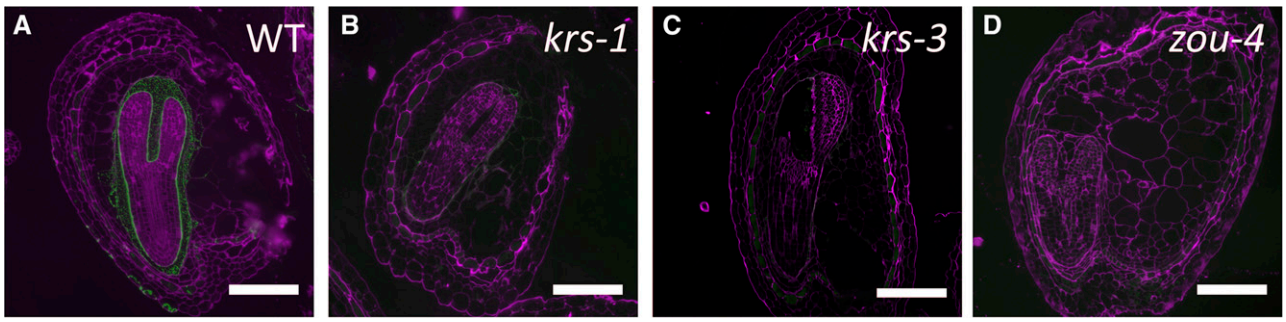


**Figure 6.** KRS Is Required for Normal Production of the Embryonic Sheath.

α-JIM12 immunolabeling of torpedo stage seed sections. Photographs show α-JIM12 labeling (green) and calcofluor labeling (magenta) of Col-0 **(A)**, *krs-1* **(B)**, *krs-3* **(C)**, and *zou-4* **(D)**. Bar = 100 μm.

2014). The *ale1-4* seedlings, which are known to be defective in embryonic cuticle formation (Tanaka et al., 2001, 2004), were used as positive controls for toluidine blue uptake in these assays. Blue coloration of the yellow etiolated cotyledon indicates a defective cuticle in qualitative assays. After treatment, wild-type cotyledons were still yellow, whereas *ale1-4* cotyledons were blue/green in color. The *krs-1*, *krs-3*, and *krs-4* mutants all showed a slight blue coloration (Figure 4B). Toluidine blue uptake quantifications were consistent with these observations, showing significant differences in uptake between wild-type cotyledons and all *krs* alleles (Figure 4C). All *krs* alleles showed the same level of toluidine blue uptake, with a slightly stronger effect observed in *ale1-4*, suggesting that KRS, like ALE1, is necessary for the formation of a normal embryonic cuticle.

Mutants defective in embryonic cuticle formation, such as *ale1-4* and *gso1-1 gso2-1*, have been reported to show an unusual seed shape phenotype (Xing et al., 2013). These phenotypes are thought to be due to abnormal adhesion between the embryo and the endosperm/testa during seed development (Tsuwamoto et al., 2008). Consistent with their weak cuticle defect, *krs* mutants had a low-penetrance seed shape phenotype (Figure 5E); 3.5% (±1.2%) of the seeds of *krs-1* were misshapen compared with 0.06% (±0.11) in the wild type. The CRISPR alleles *krs-3* and *krs-4* both produced misshapen seeds at a respective frequency of 4.5% (±0.2%) and 3.7% (±0.6%). Therefore, they are equivalent alleles in terms of seed shape phenotype penetrance. The seed-shape phenotype in *krs* mutants is not identical to that reported for *gso1-1 gso2-1* and *ale1-4* mutants. Most misshapen seeds in *krs* mutants have a twisted appearance, almost as if the embryo has been knotted (Figures 5A and 5B). Clearing of developing seeds showed that these phenotypes are due to an apparent adhesion of the embryo to the endosperm/testa in the zone of the seed furthest from the micropyle, which forces the embryo to elongate into a looped structure (Figures 5C and 5D). This is in contrast to the majority of misshapen seeds in *gso1-1 gso2-1* and *ale1-4* mutants, in which the embryo adheres to surrounding tissues at the heart stage, and therefore much nearer to the micropyle, leading to an inversion in the direction of embryo growth. In summary, the position of the embryo adhesion to surrounding tissues suggests that it may occur later in *krs* seeds (torpedo/bent cotyledon stage) than in those of *gso1-1 gso2-1* and *ale1-4* mutant seeds (heart stage).

To understand the seed phenotype of *krs* mutants in more detail, we fixed and sectioned developing seeds. In wild-type seeds, from the late heart stage, a gap is found around the embryo, caused by retraction of the endosperm during formation and permitted by the physical separation of the embryo from surrounding endosperm tissues (Figure 5F). This gap was not visible in *krs* mutants (Figure 5G) or in *zou-4* and *gso1-1 gso2-1* mutants. In *ale1-4* mutants, the gap is also less obvious than in wild-type seeds (Figures 5H to 5J). These results support the idea that that the seed shape defects in *krs* mutants, as in *gso1-1 gso2-1*, *zou-4*, and *ale1-4* mutants, are likely due to abnormal adhesion of the embryo to surrounding tissues.

One possible explanation for why the embryo and endosperm do not separate in *krs*, *gso1-1 gso2-1*, and *ale1-4* mutants is that they show a delayed endosperm cell death phenotype, as was reported in *zou* mutants. To test this possibility, we performed qRT-PCR analysis of the cell death marker *PASPA3*, which was shown to have reduced expression levels in developing *zou-4* mutant seeds (Fourquin et al., 2016). We found that although *PASPA3*, as previously reported, showed reduced expression levels in *zou-4* mutant seeds, expression levels in *krs-3* and *gso1-1 gso2-1* mutants were comparable to those in wild-type seeds, suggesting that the timing of endosperm cell death is not affected in these mutants (Supplemental Figure 8).

Interestingly, following germination, *krs* mutants have altered cotyledons that are cup-shaped, suggesting that the borders of

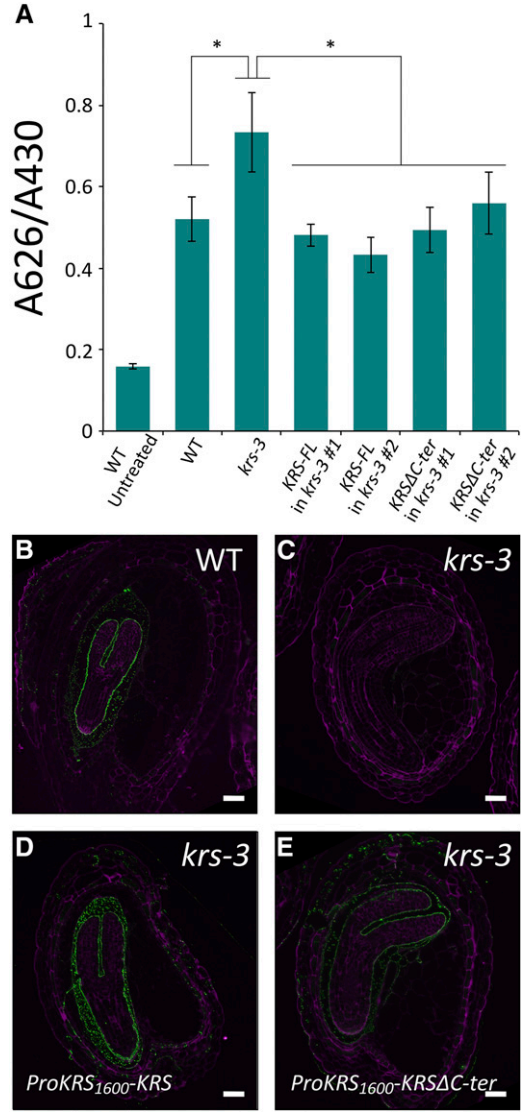


**Figure 7.** The Formation of the Embryo Sheath Is Not Dependent on the KRS C-Terminal Domain.

**(A)** Quantification of toluidine blue permeability in Col-0, *krs-3*, and *krs-3* lines transformed with *ProKRS*$_{1600}$*-KRS* (*KRS-FL*) or *ProKRS*$_{1600}$*-KRSΔC-ter*. Three biological replicates were used for each genotype. Error bars represent standard deviations. Black stars indicate statistically significant differences ($P < 0.01$) obtained after ANOVA and subsequent Tukey HSD tests. α-JIM12 immunolabeling of torpedo stage seed sections
**(B)** to **(E)** Photographs show α-JIM12 labeling (green) and calcofluor labeling (magenta) of wild-type Col-0 **(B)**, *krs-3* **(C)**, *krs-3* transformed with *ProKRS*$_{1600}$*-KRS* **(D)**, and *krs-3* transformed with *ProKRS*$_{1600}$*-KRSΔC-ter* **(E)**. Bar = 100 μm.

the cotyledon are unable to expand correctly (Figures 5K and 5L). This phenotype is observed in 40% of *krs-3* seedlings at 7 d after sowing ($n$ = 300). A similar phenotype was observed in *gso1 gso2* mutant seedlings (Tsuwamoto et al., 2008) and in *ale1-4* seedlings (Figure 5M), although at a lower frequency (20%, $n$ = 300).

### Embryo Sheath Labeling with α-JIM12 Depends on the Production of KRS

Because *KRS* encodes a peptide potentially containing a hydroxyproline-rich C-terminal domain, we tested whether the interaction of the embryo sheath with α-JIM12 would be altered in *krs* mutant seeds. We found that α-JIM12 labeling at the embryo surface and in the endosperm was dramatically reduced in *krs-1* and was absent in *krs-3* mutant seeds. This suggests that KRS contributes either directly or indirectly to the production of the epitope recognized by α-JIM12 in the embryo sheath (Figure 6). To address whether the KRS protein might act as an α-JIM12 epitope, we generated constructs expressing either a full-length version of KRS (*ProKRS$_{1600}$-KRS*) or KRS lacking the C-terminal proline-rich region (*ProKRS$_{1600}$-KRSΔC-ter*) under the *KRS* promoter in the *krs-3* mutant background. We found that both of these constructs complemented the seedling toluidine blue permeability phenotype of the *krs-3* mutant (Figure 7A). Furthermore, when we examined seeds from these lines by immunolocalization with the α-JIM12 antibody (Figures 7B to 7E), constructs in both backgrounds restored an α-JIM12 positive sheath on the embryo surface. We conclude that the C-terminal domain of KRS is not an α-JIM12 epitope during seed formation.

### *KRS* Is Not Transcriptionally Regulated by the ALE1/GSO1/GSO2 Signaling Pathway

The embryo adhesion and cuticle integrity phenotypes of *krs* mutants suggested that *KRS* could act in the same genetic pathway as *GSO1/GSO2* and *ALE1.* To test whether *KRS* expression is

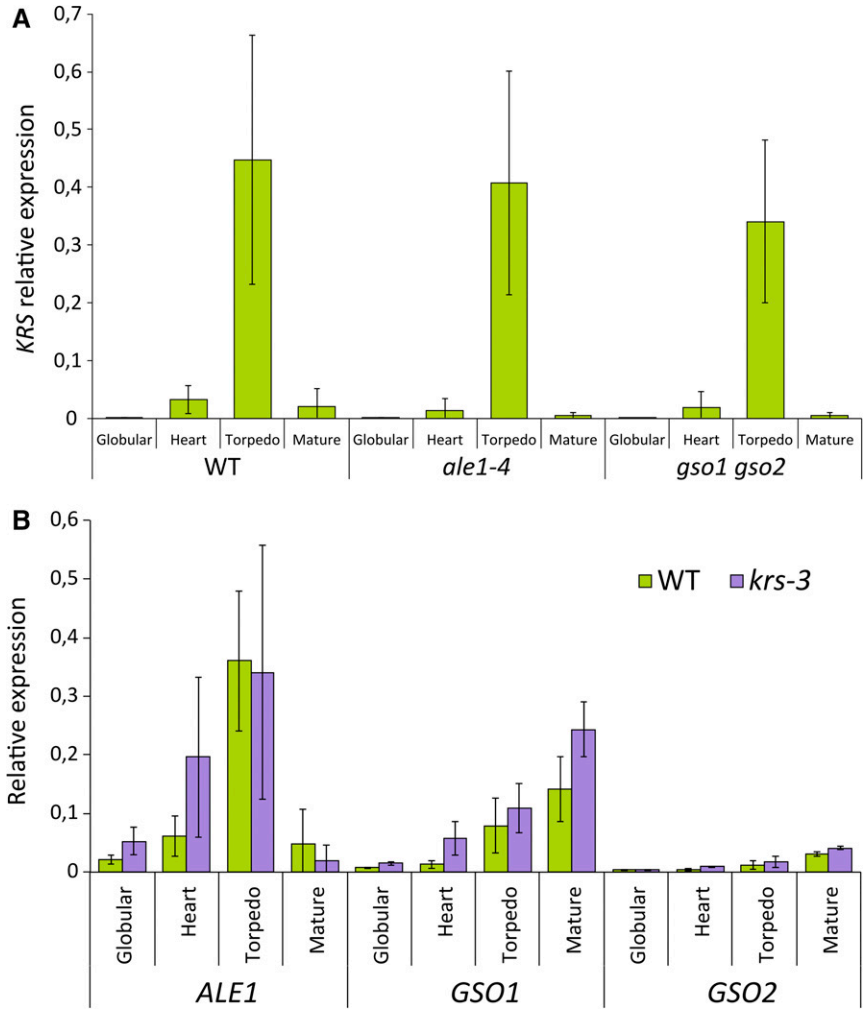


**Figure 8.** The Expression of *KRS* Is Not Affected by Loss of *ALE1*, *GSO1*, and *GSO2* Function and Vice Versa.

**(A)** *KRS* expression in Col-0, *ale1-4*, and *gso1-1 gso2-1* backgrounds at various developmental stages (globular, heart, torpedo, and mature).
**(B)** *ALE1*, *GSO1*, and *GSO2* expression in Col-0 and *krs-3* mutants. Error bars represent standard errors. Three biological replicates were used.

dependent upon the activity of *ALE1*, *GSO1*, and *GSO2*, we measured the expression levels of *KRS* in *ale1-4* and *gso1-1 gso2-1* mutant seeds (Figure 8A). Consistent with previous transcriptomic results (Xing et al., 2013), we found that *KRS* expression did not depend on the activity of either ALE1 or GSO1 and GSO2. Furthermore, the expression of *ALE1*, *GSO1*, and *GSO2* was unaltered in *krs* mutants (Figure 8B). These results suggested that *KRS* does not form part of a transcriptional cascade downstream of ALE1 GSO1 GSO2 signaling. To further understand the implication of KRS in the ALE1/GSO1/GSO2 signaling pathway, we generated triple *gso1-1 gso2-1 krs-3* mutants. These produced 100% misshapen seeds, a phenotype that could not be meaningfully quantified because *gso1 gso2* double mutant seeds are already misshapen. By contrast, a slight increase in toluidine blue permeability was observed in triple *gso1-1 gso2-1 krs-3* mutants compared with *gso1-1 gso2-1* double mutants (Figure 9A). Interestingly double *krs-3 ale1-4* mutants showed a seemingly additive seed shape phenotype, with a significantly higher proportion of misshapen seeds observed in double mutants compared with either of the two single mutants This suggested that ALE1 and KRS act in parallel to prevent adhesion between the embryo and endosperm (Figure 9B). This apparent additivity was also observed in toluidine blue permeability tests (Figure 9C). Intriguingly, we found that overexpression of the KRS protein in the endosperm of *ale1-4* mutant seeds using the promoter of the direct ZOU target *RGP3* (Denay et al., 2014) (Supplemental Figure 9) (*KRSOX*) partially suppressed the seed shape and toluidine blue permeability phenotypes observed in this background (Figures 9B to 9D).

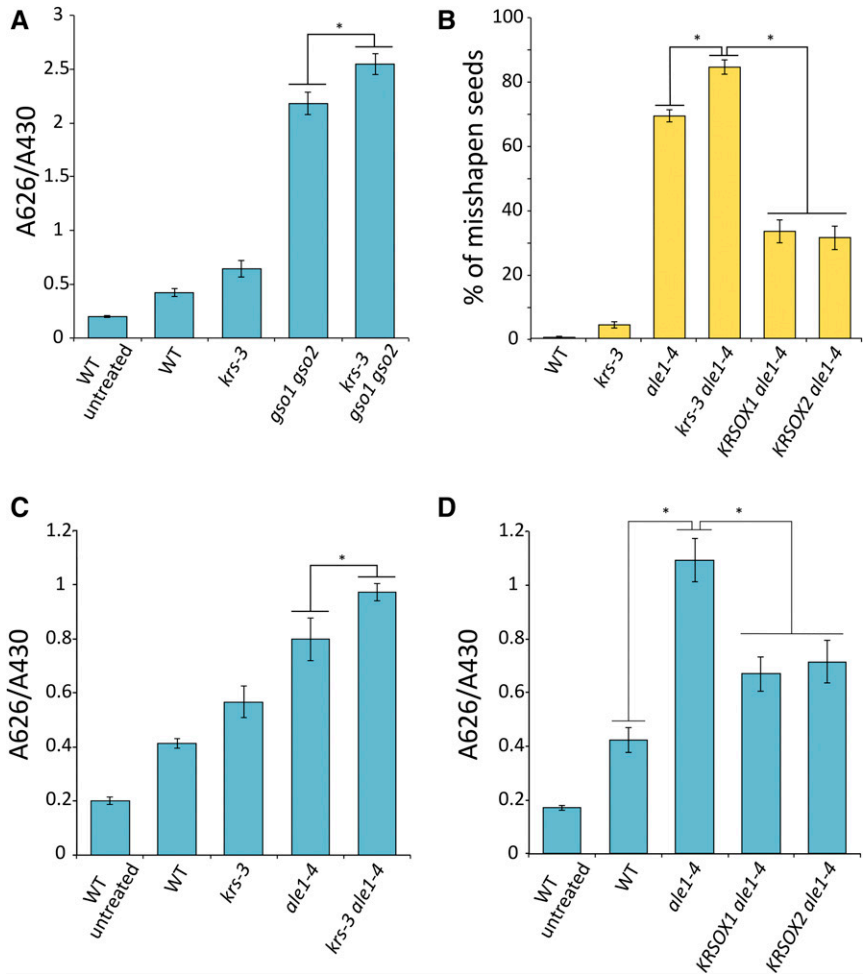


**Figure 9.** Loss of *KRS* Function Exacerbates Phenotypes Caused by Loss of *ALE1* and *GSO1 GSO2* Function.

**(A)** Toluidine blue permeability quantification in *krs-3*, *gso1-1 gso1-2*, and *krs-3 gso1-1 gso1-2* triple mutants.

**(B)** Quantification of misshapen seed phenotypes in *krs-3*, *ale1-4*, *krs-3 ale1-4* double mutants, and two *ale1-4* mutants expressing *KRS* under the control of *ProRGP3*.

**(C)** Toluidine blue permeability quantification in *krs-3*, *ale1-4*, and *krs-3 ale1-4* double mutants.

**(D)** Toluidine blue permeability quantification in *ale1* and two *ale1-4* lines expressing *KRS* under the control of *ProRGP3*.

Three biological replicates were used for each genotype. Error bars represent standard deviations. Black stars indicate statistically significant differences ($P < 0.01$) obtained after ANOVA and subsequent Tukey HSD tests.

### GSO1, GSO2, and ALE1 Affect the Deposition of the Embryo Sheath but Not the Production of α-JIM12 Epitopes in the Endosperm

To further analyze the relationship between ALE1 GSO1 GSO2 signaling and KRS function, we performed immunolocalization with *gso1-1 gso2-1* and *ale1-4* mutant seeds using the α-JIM12 antibody. Unlike *zou-4* mutants, which entirely lack labeling with α-JIM12/LM1 in the zygotic compartment, and *krs* mutants, in which the intensity of this labeling is also very strongly attenuated or absent, we found that *gso1-1 gso2-1* and *ale1-4* mutant seeds showed strong α-JIM12 labeling in the endosperm surrounding the embryo (Figure 10; Supplemental Figure 10). In *ale1-4* mutant seeds, labeling of the embryo sheath was similar to that observed in the wild type, although it was occasionally diffuse and patchy, especially in the cotyledons, whereas in *gso1-1 gso2-1* mutant seeds, no labeling was detected at the embryo surface, and the signal was localized to the cells of the embryo surrounding endosperm, within an apparently vesicular compartment. These results suggest that GSO1 and GSO2, and to a lesser extent ALE1, function to mediate the deposition of the embryo sheath on the embryonic surface.

## DISCUSSION

We have presented ultrastructural, phenotypic, and genetic data showing that the plant-specific peptide KRS plays an important role in the formation of a structure we have termed the embryo sheath, at the embryo surface. We show that KRS is necessary for the production of a component of this structure that reacts strongly with the antiextensin antibody α-JIM12. However, although we demonstrate correlation between the expression of *KRS* (spatially, temporally, and in the various mutant backgrounds investigated) and the production of α-JIM12-reactive material in the developing endosperm, our complementation experiments suggested that the C-terminal domain of KRS is not an α-JIM12 epitope. Our results suggest that the activity of KRS leads indirectly to the production of the α-JIM12 epitope, the source of which remains unidentified.

Based on the presence of a clearly defined predicted secretion signal, KRS likely encodes a secreted protein. Another family member, tomato STIG1 protein, was secreted from stigmatic tissues and bound to the surface of invading pollen tubes, promoting their growth (Huang et al., 2014; Tang et al., 2004). Our data showed that KRS is required for the production of an extracellular structure, which coats the developing embryo. This suggests that material is actively secreted by the endosperm onto the embryo surface. Although such a secretion activity has not yet been described in detail in Arabidopsis, ultrastructural studies of the developing seeds of black nightshade (*Solanum nigrum*) and maize (*Zea mays*) have produced images suggestive of active and directional secretion of material from the endosperm via large vesicles (Briggs, 1993, 1996; Schel et al., 1984), although the identity of this material remains unclear. Because lack of sheath production correlates with adhesion of the embryo and endosperm, one possibility is that the sheath is composed of a glycoprotein-rich slime or mucilage that lubricates the movement of the embryo through the endosperm. However, testing this hypothesis is technically challenging.

Solanaceous STIG1 proteins are processed during or after secretion in tomato, tobacco, and petunia, so that both the N-terminal secretion signal and the nonconserved domain of the protein are lost, leading to the production of a mature peptide containing the conserved cysteine-rich STIG1 domain (Huang et al., 2014; Verhoeven et al., 2005). STIG1 appears to stimulate pollen tube growth in vivo (Huang et al., 2014; Tang et al., 2004). Importantly, this stimulation is dependent upon the expression of the POLLEN-SPECIFIC RECEPTOR-LIKE KINASE2 (Le-PRK2), whose extracellular domain binds directly to the STIG1 protein, leading to increased redox potential in growing pollen tubes. Thus, the STIG1 domain is likely a functional ligand for Le-PRK2. Interaction of STIG1 with the extracellular domain of Le-PRK2 has been shown to depend upon specific amino acids within the conserved cysteine-rich domain of STIG1. The STIG1 domain of tomato STIG1 also mediates interaction with phosphatidylinositol-3-phosphate at the pollen-tube surface, an interaction that is also required for the stimulation of pollen tube growth (Huang et al., 2014). Another member of this class of peptides, GRIM

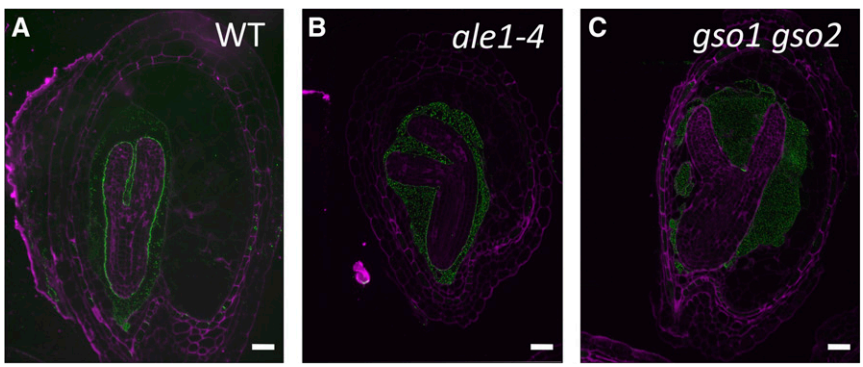


**Figure 10.** Embryo Sheath Material Is Not Deposited Normally on the Surface of *ale1-4* and *gso1-1 gso2-1* Mutant Embryos.

α-JIM12 immunolabeling (green) and calcofluor counterstaining (magenta) in Col-0 **(A)**, *ale1-4* **(B)**, and *gso1 gso2* **(C)**. Images showing calcofluor staining alone are shown in Supplemental Figure 10. Bar = 50 μm.

REAPER (GRI) has also been shown to act as a ligand for an RLK, although it was shown that an 11-amino acid peptide produced by AtMETACASPASE-9-mediated processing of the nonconserved N-terminal domain that was shown to bind the extracellular domain of the Arabidopsis PRK5 (Wrzaczek et al., 2015). This association triggers ion leakage and cell death. The PRK5 ligand domain of GRI is not conserved either in KRS or other Arabidopsis family members.

The fact that both STIG1 and GRI are processed to form RLK ligands raises the question of whether KRS, or a processed product of KRS, could also act as an RLK ligand. An obvious possibility is that KRS could act as a ligand in the signaling pathway comprising the RLKs GSO1/GSO2 and the subtilisin protease ALE1. Therefore, we tested the genetic interactions of *KRS* with the components of this pathway, which is known to be involved in ensuring the production of a functional embryonic cuticle. We summarized our findings in the model shown in Figure 11. Based on our results, the possibility that KRS acts as a ligand for GSO1 and GSO2, and/or that KRS is an ALE1 substrate, cannot formally be excluded. However, the expression of *KRS* initiates relatively late in seed development compared with that of *ALE1.*

More importantly, we found that the phenotypic consequences of loss of *KRS* function, in terms of production of embryonic sheath material, were not identical to those of *ale1* and *gso1 gso2* mutants. We found that KRS, unlike ALE1 and GSO1/GSO2, was involved in the production of α-JIM12 antigen in the endosperm. By contrast, GSO1 and GSO2, and to a lesser extent ALE1, were necessary for the deposition of material containing the α-JIM12 antigen on the embryo surface. In this context, it is particularly interesting to note the high penetrance of the cupped cotyledon phenotype in *krs* mutants compared with *ale1* mutants. This phenotype may be a consequence of the abnormal adhesion of endosperm material to the surface of the cotyledons (as we observed in *zou* mutants), which could mechanically constrain the expansion of the cotyledon boundaries (Yang et al., 2008). The *krs* mutants show a significantly stronger cotyledon cupping phenotype than do *ale1* mutants, and this correlates with the stronger sheath and separation phenotype observed in *krs* mutants at the cytological level. Consistent with this idea, the cotyledon cupping phenotype is also prevalent in *gso1 gso2* double mutants (Tsuwamoto et al., 2008), in which the release of sheath materials onto the embryonic surface is completely absent. Consistent with the differences described above, the seed shape phenotype of *krs* mutants is also not identical to that of *ale1* and *gso1 gso2* mutants, but is suggestive of adhesion events that occur later in seed development.

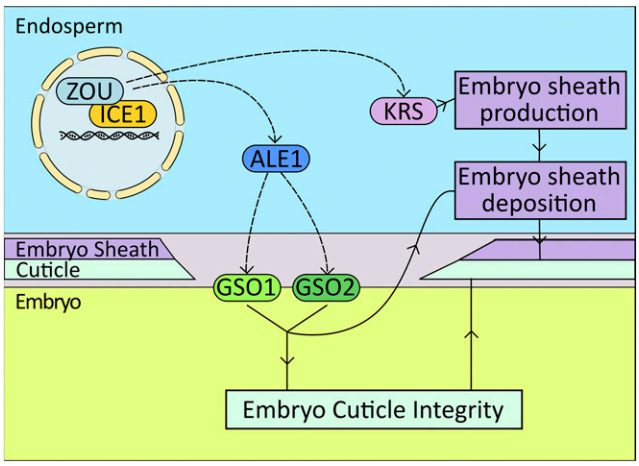


**Figure 11.** Schematic Summary of Conclusions from This Work.

Regulatory/genetic relationships are shown as hashed lines, and functional relationships are shown as continuous lines. The ZOU transcription factor, expressed exclusively in the endosperm, acts as a heterodimer with ICE1 and regulates the expression of both the subtilisin protease ALE1 and the peptide KRS in the endosperm. ALE1 acts in the same pathway as the GSO1 and GSO2 receptor-like kinases to ensure normal embryonic cuticle formation. In parallel, KRS is necessary for the production of embryo sheath material in endosperm cells surrounding the embryo. Finally, the activities of GSO1, GSO2, and ALE1 are necessary for the deposition of sheath material on the surface of the developing embryo.

Our phenotypic and cytological data, taken together with the apparently additive genetic interaction observed between *krs* and *ale1* mutants, suggest that KRS acts in parallel with ALE1, GSO1, and GSO2. In this model, KRS is necessary for embryo sheath production and, therefore, for preventing abnormal adhesion of the embryo as it grows through the degenerating endosperm. Adhesions could cause tearing of the embryo cuticle, which might explain toluidine blue permeability in the *krs* embryo. Cuticle permeability and seed shape defects in *ale1* mutants were more pronounced than those of *krs* mutants, whereas sheath deposition was less strongly affected, suggesting that embryo adhesions and cuticle defects in *ale1* mutants are not solely attributable to defects in the embryo sheath. Nonetheless, our observation that overexpression of KRS in the *ale1-4* mutant endosperm leads to an alleviation of the *ale1* seed phenotype is intriguing and suggests some overlap between the functions of ALE1 and KRS. In this context, the total lack of sheath deposition in *gso1 gso2* mutants is a particularly interesting phenotype and suggests that GSO1 and GSO2 act downstream of both ALE1 (in preventing early embryo adhesion and cuticle permeability) and KRS (in terms of the production of a functional sheath). Understanding the molecular basis for this apparent dual function will shed considerable light on endosperm/embryo interactions. More generally, how the process of cuticle deposition affects, or is affected by, sheath formation remains a particularly important subject for further investigation.

Although the expression of *KRS* and *ALE1* in the developing endosperm is mutually independent, the expression of both genes depends upon the activity of the ZOU/ICE1 transcription factor complex in the seed (Yang et al., 2008). However, we have not been unable to show direct binding of ZOU/ICE1 heterodimers to the promoters of either *KRS* or *ALE1*, suggesting that their regulation is likely indirect. For *ALE1*, this idea is further supported by expression observed during very early seed development in *zou* mutant seeds at stages before ZOU protein fusions can be detected in wild-type seeds (Xing et al., 2013; Yang et al., 2008). Such expression is not observed for the direct ZOU target *RGP3*, whose expression is never detected in the endosperm of *zou* mutants (Denay et al., 2014; Fourquin et al., 2016). *KRS* expression in the root, where ZOU is never expressed (Yang et al., 2008), supports the idea that regulation is not necessarily directly ZOU dependent.

The basis for ZOU/ICE1 regulation of the expression of these genes thus also remains to be resolved, although it may be associated with cell wall thinning functions of ZOU in the endosperm that eventually lead to endosperm disintegration and death (Fourquin et al., 2016).

## METHODS

### Plant Materials and Growth Conditions

All plant materials used in the project were in the *Arabidopsis thaliana* Columbia (Col-0) background. Several genotypes described in the work have been previously published as follows: *zou-4* (Yang et al., 2008), *ale1-4* (Xing et al., 2013), and *gso1-1 gso2-1* (Tsuwamoto et al., 2008). *krs-1* is a T-DNA insertion allele (GABI_824G07) from the GABI-Kat collection (Kleinboelting et al., 2012) and was obtained from the Nottingham Arabidopsis Stock Centre (NASC). CRISPR alleles of *KRS* were obtained as described below. Genotyping of *krs* mutants was performed using primers listed in Supplemental Table 1

Unless otherwise specified, chlorine gas-sterilized seeds were sown on Murashige and Skoog (MS) agar plates with 0.5% sucrose, stratified for 2 d in the dark at 4°C, grown under long-day conditions (21°C, 16 h light/8 h dark) for 10 d, and then transferred to soil under standard long-day conditions (21°C, 16 h light/8 h dark). To obtain synchronous seed material, newly opened flowers were marked with threads each day for 2 weeks.

For toluidine blue staining of etiolated seedlings, chlorine gas-sterilized seeds were spread uniformly on 15-cm MS plates containing 0.5% sucrose and 0.4% Phytagel (Sigma-Aldrich) (pH 5.8) and stratified for 2 d in the dark at 4°C. Following stratification, seeds were transferred to a growth chamber and incubated for 6 h under continuous light followed by 4 d in the dark. For toluidine blue assays, seedlings were not returned to the dark, and were grown for 10 d prior to assaying as described (Xing et al., 2013).

### Statistical Analysis of Toluidine Blue Permeability and Seed Shape Phenotypes

For quantified toluidine blue permeability assays, at least three independent biological replicates of seeds from concomitantly grown plants were used for each genotype. Data were subjected to an ANOVA test, and where differences were detected, a Tukey HSD test was used to whether significant differences existed between specific genotypes.

To quantify seed shape defects, populations of seeds from independent, concomitantly grown plants were photographed and visually scored. At least three independent samples were used for each genotype, and at least 300 seeds were scored per independent plant. Data were subjected to an ANOVA test, and where differences were detected, a Tukey HSD test was used to whether significant differences existed between specific genotypes.

### Generation of Phylogenetic Trees

Phylogenetic analysis was performed as follows. Amino acid sequence alignments were generated with the Muscle algorithm (Edgar, 2004). Sequences were curated using Gblocks (Castresana, 2000) under low stringency conditions, which allow smaller final blocks, gap positions with the final blocks, and less strict flanking positions. Phylogenetic trees were built using PhyML 3.0 (Guindon et al., 2010), with aLRT (SH-like) for branch support, model-derived amino acid equilibrium frequencies, optimized invariable sites, and optimized across-site rate variation. Tree searching was performed using BEST (best of NNI and SPR). The starting tree was generated using BIONJ with an optimized tree topology.

### Generation of New *KRS* Alleles Using CRISPR/Cas9 Technology

Independent CRISPR edited *krs* alleles were generated using two different strategies. The *krs-3* allele was generated using the protocol and vectors described by Schiml et al. (2016), and the *krs-4* allele was generated using the protocol and vectors described by Peterson et al. (2016). For *krs-3*, *pDE-CAS9-crikrs1*, the *CRISPR-Cas9*-containing vector used to induce the mutation, was generated as follows. The *5′-CAAACGGTCCGGACCATCAG-3′* PAM sequence was cloned by restriction into the *pEN-Chimera* vector (Schiml et al., 2016), giving the *pEN-Chimera-crikrs1* vector. Gateway LR recombination was then performed using *pEN-Chimera-cri1* and *ProDE-Cas9*, to produce the plant transformation vector *pDE-Cas9-crikrs1*. For *krs-4*, the *5′-ACTTAACA-CAACCTCGTCA-3′* PAM sequence was cloned into the *pCUT*3 vector (Peterson et al., 2016), resulting in the plant expression vector *CUT3-crikrs2*. Both vectors were transformed into the Col-0 background. Primary transformants were generated and screened for the presence of gene editing by amplifying *KRS* genomic DNA with *KRS_F* and *KRS_R*, and sequencing the resulting PCR products using the using the *KRScriSeq* primer. Homozygous plants were identified in the T2 generation using the same technique. Primer sequences are shown in Supplemental Table 1. To remove the Cas9-encoding cassette, homozygous plants were backcrossed to Col-0, and homozygous mutant lines lacking the Cas9 cassette were identified by lack of resistance to appropriate antibiotics. The absence of the Cas9 cassette was verified by PCR using the primers *SS42* and *SS43* (Supplemental Table 1)

### Generation of Other Transgenic Lines

The *ProKRS$_{1600}$-VN7*, *ProKRS$_{4000}$-VN7*, and *ProRGP3-VN7* lines were generated in the Col-0 background, and the *ProKRS$_{1600}$-KRS* and *ProKRS$_{1600}$-KRSΔC-ter* constructions were transformed directly into the *krs-3* mutant background. The expression vector containing the *ProKRS$_{1600}$-VN7*, *ProKRS$_{4000}$-VN7*, and *ProRGP3-VN7* constructs were produced as follows. The 1600- and 4000-bp upstream sequences of *KRS* were amplified using the primers listed in Supplemental Table 1. They were cloned by restriction with *Xho*I and *Bam*HI into the *pENTR5′-MCS* vector (Creff et al., 2015). For *ProRGP3-VN7*, a 439-bp promoter upstream of the *RGP3* open reading frame was amplified using the primers listed in Supplemental Table 1. The product was recombined into *pDONR P4-P1r* (Invitrogen) to give *pENTR5′-ProRGP3.* Triple LR reactions were performed using *pENTR5′-pKRS$_{1600}$*, *pENTR5′-pKRS$_{4000}$*, or *pENTR5′-ProRGP3* in combination with *pENTRgene-VENUS-N7*, *pENTR3′-Mock*, and the *pBART* (Gleave, 1992) destination vector. The *ProKRS$_{1600}$-KRS* and *ProKRS$_{1600}$-KRSΔC-ter* constructs were produced as follows: PCR products harboring attB borders were generated from genomic DNA using primers *krs_F_attB1* and *krs_R_attB2* for *KRS* or *krs_F_attB1* and *krs_R_ΔC-ter_attB2* for *KRSΔC-ter.* BP reactions were performed with the pDONR221 vector to generate the *pENTRg-KRS* and *pENTRg-KRSΔC-ter* vectors. Finally, triple LR reactions were performed using *pENTRg-KRS* or *pENTRg-KRSΔC-ter* in combination with *pENTR5′-ProKRS$_{1600}$*, *pENTR3′-Mock*, and the *pBART* destination vector.

The resulting plant expression vectors were transformed into plants using *Agrobacterium tumefaciens*-mediated plant transformation using the floral dip method (Logemann et al., 2006), and at least four independent transformation events were analyzed for each line.

### In Situ Hybridization

The DNA template was amplified from *KRS gDNA* using *KRS_F* and *KRS_R* primers and subsequently cloned into *pTOPO* ZeroBlunt vector (Invitrogen). The *KRS* antisense probe was amplified from genomic DNA using *KRS_F* and *SP6* primers (Supplemental Table 1). Digoxigenin-labeled RNA probes were produced and hybridized to tissue sections. Siliques were opened, fixed overnight in ice-cold PBS containing 4% paraformaldehyde, dehydrated through an ethanol series, and embedded in Paraplast Plus (McCormick Scientific). Eight-micrometer sections were cut and immobilized on coated slides (Menzel-Gläzer Superfrost Ultra Plus$^{R}$; Thermo Scientific). Sections were dewaxed and hydrated, treated

with 2× saline sodium citrate (20 min), and digested for 15 min at 37°C with proteinase K (20 mg/mL) in 50 mM Tris-HCl, pH 7.5, and 5 mM EDTA. Samples were then treated for 2 min with 0.2% glycine in PBS, rinsed, postfixed with 4% paraformaldehyde in PBS (10 min, 4°C), rinsed, treated with 0.25% (w/v) acetic anhydride in 100 mM triethanolamine (pH 8.0 with HCl) for 10 min, rinsed, and dehydrated. Sections were then hybridized under cover slips overnight at 50°C with RNA probes (produced using DIG RNA labeling kit; Roche) diluted in DIG Easy Hyb solution (Roche) following the manufacturer's instructions. Following hybridization, the slides were extensively washed in 0.1× saline sodium citrate and 0.5% SDS at 50°C (3 h), blocked for 1 h in 1% blocking solution (Roche) in TBS and for 30 min in BSA solution (1% BSA, 0.3% Triton X-100, 100 mM Tris-HCl, 100 mM NaCl, and 50 mM $MgCl_2$), and then incubated in a 1/3000 dilution of in alkaline phosphatase-conjugated antidigoxigenin antibody (Roche; lot 11266026) in BSA solution for 2 h at room temperature. Sections were extensively washed in BSA solution, rinsed, and treated overnight in the dark with a buffered NBT/BCIP solution. Samples were rinsed in water before air drying and mounting in Entellan (Sigma-Aldrich).

### Microscopy

Developing live seeds were imaged by opening siliques and removing the internal connecting tissue, with seeds attached, into a drop of water. Seeds were then gently covered with a cover slip. Roots were imaged by coloring with propidium iodide (1 μg/mL) (Sigma-Aldrich) and mounting in water. Embryos were imaged by gently bursting seeds between a slide and a cover slip in water. Confocal imaging was performed using a Zeiss LSM700 and a LSM710. Light/fluorescence microscopy imaging was performed using a Zeiss Axioimager 2. Photographs of dry seeds and seedlings were obtained using a Leica MZ12 dissection microscope fitted with an AxioCamICc5.

### Quantitative Gene Expression Analysis Using qRT-PCR

Intact siliques were frozen in liquid nitrogen and total RNA was extracted using the Spectrum Plant Total RNA Kit (Sigma-Aldrich). Total RNAs were digested with Turbo DNA-free DNase I (Ambion) according to the manufacturer's instructions. RNA was reverse transcribed using the SuperScript VILO cDNA synthesis kit (Invitrogen) according to the manufacturer's protocol. PCR reactions were performed in an optical 384-well plate in the QuantStudio 6 Flex System (Applied Biosystems), using FastStart Universal SYBR Green Master (Rox) (Roche), in a final volume of 10 μL, according to the manufacturer's instructions. The following standard thermal profile was used for all PCR reactions: 95°C for 10 min, 40 cycles of 95°C for 10 s, and 60°C for 30 s. Data were analyzed using the QuantStudio 6 Flex Real-Time PCR System Software (Applied Biosystems). As a reference, primers for the *EIF4A* cDNA were used. PCR efficiency (E) was estimated from the data obtained from standard curve amplification using the equation $E = 10^{-1/slope}$. Expression levels are presented as $E^{-\Delta Ct}$, where $\Delta Ct = Ct_{GOI}-Ct_{EIF4A}$. Primers are listed in Supplemental Table 1. *PASPA3* primers are described by Fourquin et al. (2016). All qRT-PCR experiments were performed using three independent biological replicates.

### Immunofluorescent Labeling of Seeds

Single seeds were fixed in ice-cold PEM buffer (50 mM PIPES, 5 mM EGTA, and 5 mM $MgSO_4$, pH 6.9) containing 4% (w/v) paraformaldehyde. Samples were placed under vacuum to encourage penetration of fixative (3 × 30 min on ice), rinsed in PBS, dehydrated through an ethanol series, and infiltrated with increasing concentrations of LR White resin in absolute ethanol (London Resin Company) over 8 d before being polymerized in 100% resin in Beem capsules (Electron Microscopy Sciences) at 60°C. The 1.0-μm sections were cut using a glass knife on a Leica RM6626 microtome. Sections were incubated in PBS containing 3% (w/v) milk protein and a 10-fold dilution of antibody hybridoma supernatant (Molecular Probes) for 1 h, washed, and incubated with a 100-fold dilution of fluorescein-linked secondary antibody (Abcam anti-Rat IgM; ab96963) for 1 h in the dark. Samples were washed and cell walls were counterstained with filtered Calcofluor White M2R, which binds to cellulose and chitin (fluorescent brightener 28; Sigma-Aldrich) at 0.25 μg $mL^{-1}$ and mounted in Vectashield (Eurobio).

### Immunogold Labeling

Single seeds were fixed by high-pressure freeze substitution using an EM PACT1 device (Leica Microsystems) with a carrier depth of 200 μm. Single seeds were dissected, deposited in the carrier filled with BSA 20% (w/v) in 0.5× MS, and immediately frozen. Freeze substitution was performed in acetone containing 0.5% glutaraldehyde, 0.1% uranyl acetate, and 2% $OsO_4$ at –90°C for 48 h followed by a temperature ramp of 3°C per hour to −50°C. Samples were washed three times with 100% acetone and three times with 100% ethanol. Samples were infiltrated with Lowicryl HM20 resin at −50°C (2 h at 25%, 2 h at 50%, overnight at 75%, 3 × 2 h at 100%). Polymerization was performed progressively under UV illumination for 48 h at −50°C followed by 48 h at 20°C.

Ultrathin (90 nm) sections were made with a Leica UC7 ultramicrotome and placed on grids. Grids were placed on 30 μL drops of filtered water (for 2 × 5 min), and then PBSTB (1× PBS, 0.2% Tween, and 1% BSA) for 15 min. Grids were then transferred to 20 μL drops of PBSTB containing a 1:10 dilution of antibody hybridoma supernatant (Molecular Probes) for 1 h. Grids were washed on 30 μL drops of PBSTB (for 4 × 5 min). Grids were then transferred to 20 μL drops of PBSTB containing a 1:30 dilution of 10-nm gold-linked anti-rat secondary antibody (Tebu, biocell, ref: EM-GAR10, lot 08721) for 1 h. Grids were washed on 30-μL drops of PBSTB (for 4 × 5 min). Grids were then transferred to 20-μL drops of 0.1% glutaraldehyde for 1 min before washing with 30-μL drops of filtered water (for 4 × 5 min). Grids were imaged at 120 kV using an FEI TEM Tecnai Spirit with 4k × 4k eagle CCD.

### Accession Numbers

Sequence data from this article can be found in the GenBank/EMBL data libraries under the following accession numbers: *KRS*, AT1G50650; *ZOU*, AT1G49770; *ALE1*, AT1G62340; *GSO1*, AT4G20140; and *GSO2*, AT5G44700. Germplasm included the following: *krs-1*, GABI_824G07; *krs-2*, SALK_115353; *zou-4*, GK-584D09; *ale1-4*, SAIL_279_C04; *gso1-1*, SALK_064029; and *gso2-1*, SALK_130637.

### Supplemental Data

**Supplemental Figure 1.** Fluorescent Immunolocalization Experiments Using the α-LM1 Antibody.

**Supplemental Figure 2.** TEM Images of Immunogold Labeling with the α-LM1 Antibody and Negative Control.

**Supplemental Figure 3.** KRS Phylogenetic Analyses.

**Supplemental Figure 4.** *KRS* in Silico Expression Data.

**Supplemental Figure 5.** *KRS* Promoter Activity in the Root.

**Supplemental Figure 6.** Expression of *KRS* Relative to Expression of *EIF4* in Col-0 and *krs-1* Mutant Seeds at Various Developmental Stages.

**Supplemental Figure 7.** Alignment of *KRS* cDNA and Predicted Encoded Protein Sequences for Wild-Type and New *krs* Alleles.

**Supplemental Figure 8.** Loss of KRS or GSO1 and GSO2 Function Does Not Lead to a Delay in Endosperm Cell Death.

**Supplemental Figure 9.** Expression of the *RGP3* Promoter Is Restricted to the Endosperm in Developing Seeds.

**Supplemental Figure 10.** Endosperm Structure in the Wild Type, *ale1-4*, and *gso1 gso2* Mutants.

**Supplemental Table 1.** Primers Used in This Study.

**Supplemental File 1.** ANOVA Tables.

**Supplemental File 2.** Text File of the Sequences and Alignment Used for the Phylogenetic Analysis Shown in Supplemental Figure 3A.

## ACKNOWLEDGMENTS

We thank the European Arabidopsis Stock Centre (NASC) for providing seed. We thank Holger Puchta (University of Karlsruhe) for providing published CRISPR vectors and the plant culture and logistics and secretarial teams at the Laboratoire Reproduction et Développement des Plantes for their invaluable support. This work was financed by a grant to G.I. from the Agence Nationale de la Recherche (ANR-13-BSV2-0002, INASEED), by a doctoral grant from the Region Rhône-Alpes, and by grants to Z.L.N. from the National Science Foundation (IOS-1455607).

## AUTHOR CONTRIBUTIONS

G.I. conceived the project. G.I. and S.M. designed the experiments. G.I. and T.W. supervised the experiments. S.M. performed most of the experiments with help from N.M.D., S.C., and C.F. S.M., N.M.D., and G.I. analyzed the data. S.C. and A.C. provided technical assistance to S.M. and G.I. Z.L.N. provided a construct for CRISPR experiments. L.B. carried out immunogold labeling experiments. S.M. and G.I. wrote the article with contributions from all the authors.

Received January 10, 2017; revised May 23, 2017; accepted July 9, 2017; published July 10, 2017.

## REFERENCES

**Berger, F.** (2003). Endosperm: the crossroad of seed development. Curr. Opin. Plant Biol. **6:** 42–50.

**Brady, S.M., Orlando, D.A., Lee, J.-Y., Wang, J.Y., Koch, J., Dinneny, J.R., Mace, D., Ohler, U., and Benfey, P.N.** (2007). A high-resolution root spatiotemporal map reveals dominant expression patterns. Science **318:** 801–806.

**Briggs, C.L.** (1996). An ultrastructural study of the embryo/endosperm interface in the developing seeds of *Solanum nigrum* L. zygote to mid torpedo stage. Ann. Bot. (Lond.) **78:** 295–304.

**Briggs, C.L.** (1993). Endosperm development in *Solanum nigrum* L. formation of the zone of separation and secretion. Ann. Bot. (Lond.) **72:** 303–313.

**Castresana, J.** (2000). Selection of conserved blocks from multiple alignments for their use in phylogenetic analysis. Mol. Biol. Evol. **17:** 540–552.

**Cheung, A.Y., Boavida, L.C., Aggarwal, M., Wu, H.-M., and Feijó, J.A.** (2010). The pollen tube journey in the pistil and imaging the in vivo process by two-photon microscopy. J. Exp. Bot. **61:** 1907–1915.

**Creff, A., Brocard, L., and Ingram, G.** (2015). A mechanically sensitive cell layer regulates the physical properties of the Arabidopsis seed coat. Nat. Commun. **6:** 6382–6389.

**Delude, C., Moussu, S., Joubès, J., Ingram, G., and Domergue, F.** (2016). Plant surface lipids and epidermis development. In Lipids in Plant and Algae Development, Y. Nakamura and Y. Li-Beisson, eds (Cham, Switzerland: Springer International Publishing), pp. 287–313.

**Denay, G., Creff, A., Moussu, S., Wagnon, P., Thévenin, J., Gérentes, M.-F., Chambrier, P., Dubreucq, B., and Ingram, G.** (2014). Endosperm breakdown in Arabidopsis requires heterodimers of the basic helix-loop-helix proteins ZHOUPI and INDUCER OF CBP EXPRESSION 1. Development **141:** 1222–1227.

**Edgar, R.C.** (2004). MUSCLE: multiple sequence alignment with high accuracy and high throughput. Nucleic Acids Res. **32:** 1792–1797.

**Fourquin, C., Beauzamy, L., Chamot, S., Creff, A., Goodrich, J., Boudaoud, A., and Ingram, G.** (2016). Mechanical stress mediated by both endosperm softening and embryo growth underlies endosperm elimination in Arabidopsis seeds. Development **143:** 3300–3305.

**Gleave, A.P.** (1992). A versatile binary vector system with a T-DNA organisational structure conducive to efficient integration of cloned DNA into the plant genome. Plant Mol. Biol. **20:** 1203–1207.

**Guindon, S., Dufayard, J.-F., Lefort, V., Anisimova, M., Hordijk, W., and Gascuel, O.** (2010). New algorithms and methods to estimate maximum-likelihood phylogenies: assessing the performance of PhyML 3.0. Syst. Biol. **59:** 307–321.

**Huang, W.-J., Liu, H.-K., McCormick, S., and Tang, W.-H.** (2014). Tomato pistil factor STIG1 promotes in vivo pollen tube growth by binding to phosphatidylinositol 3-phosphate and the extracellular domain of the pollen receptor kinase LePRK2. Plant Cell **26:** 2505–2523.

**Ingram, G.C.** (2010). Family life at close quarters: communication and constraint in angiosperm seed development. Protoplasma **247:** 195–214.

**Kleinboelting, N., Huep, G., Kloetgen, A., Viehoever, P., and Weisshaar, B.** (2012). GABI-Kat SimpleSearch: new features of the *Arabidopsis thaliana* T-DNA mutant database. Nucleic Acids Res. **40:** D1211–D1215.

**Kondou, Y., Nakazawa, M., Kawashima, M., Ichikawa, T., Yoshizumi, T., Suzuki, K., Ishikawa, A., Koshi, T., Matsui, R., Muto, S., and Matsui, M.** (2008). RETARDED GROWTH OF EMBRYO1, a new basic helix-loop-helix protein, expresses in endosperm to control embryo growth. Plant Physiol. **147:** 1924–1935.

**Lamport, D.T.A.** (1973). The role of hydroxyproline-rich proteins in the extracellular matrix of plants. Symp. Soc. Dev. Biol. Symp. **30:** 113–130.

**Le, B.H., et al.** (2010). Global analysis of gene activity during Arabidopsis seed development and identification of seed-specific transcription factors. Proc. Natl. Acad. Sci. USA **107:** 8063–8070.

**Lee, K.J.D., Dekkers, B.J.W., Steinbrecher, T., Walsh, C.T., Bacic, A., Bentsink, L., Leubner-Metzger, G., and Knox, J.P.** (2012). Distinct cell wall architectures in seed endosperms in representatives of the Brassicaceae and Solanaceae. Plant Physiol. **160:** 1551–1566.

**Li, J., and Berger, F.** (2012). Endosperm: food for humankind and fodder for scientific discoveries. New Phytol. **195:** 290–305.

**Liu, X., Wolfe, R., Welch, L.R., Domozych, D.S., Popper, Z.A., and Showalter, A.M.** (2016). Bioinformatic identification and analysis of extensins in the plant kingdom. PLoS One **11:** e0150177.

**Logemann, E., Birkenbihl, R.P., Ülker, B., and Somssich, I.E.** (2006). An improved method for preparing Agrobacterium cells that simplifies the Arabidopsis transformation protocol. Plant Methods **2:** 16.

**Olsen, O.-A.** (2004). Nuclear endosperm development in cereals and Arabidopsis thaliana. Plant Cell **16** (suppl.): S214–S227.

**Peterson, B.A., Haak, D.C., Nishimura, M.T., Teixeira, P.J.P.L., James, S.R., Dangl, J.L., and Nimchuk, Z.L.** (2016). Genome-wide assessment of efficiency and specificity in CRISPR/Cas9 mediated multiple site targeting in Arabidopsis. PLoS One **11:** e0162169.

**Schel, J.H.N., Kieft, H., and Lammeren, A.A.M.V.** (1984). Interactions between embryo and endosperm during early developmental stages of maize caryopses (*Zea mays*). Can. J. Bot. **62:** 2842–2853.

**Schiml, S., Fauser, F., and Puchta, H.** (2016). CRISPR/Cas-mediated site-specific mutagenesis in *Arabidopsis thaliana* using Cas9 nucleases and paired nickases. In Chromosome and Genomic Engineering in Plants, M. Murata, ed (New York: Springer), pp. 111–122.

**Shi, S.-P., Chen, X., Xu, H.-D., and Qiu, J.-D.** (2015). PredHydroxy: computational prediction of protein hydroxylation site locations based on the primary structure. Mol. Biosyst. **11:** 819–825.

**Smallwood, M., Beven, A., Donovan, N., Neill, S.J., Peart, J., Roberts, K., and Knox, J.P.** (1994). Localization of cell wall proteins in relation to the developmental anatomy of the carrot root apex. Plant J. **5:** 237–246.

**Smallwood, M., Martin, H., and Knox, J.P.** (1995). An epitope of rice threonine- and hydroxyproline-rich glycoprotein is common to cell wall and hydrophobic plasma-membrane glycoproteins. Planta **196:** 510–522.

**Tanaka, H., Onouchi, H., Kondo, M., Hara-Nishimura, I., Nishimura, M., Machida, C., and Machida, Y.** (2001). A subtilisin-like serine protease is required for epidermal surface formation in Arabidopsis embryos and juvenile plants. Development **128:** 4681–4689.

**Tanaka, T., Tanaka, H., Machida, C., Watanabe, M., and Machida, Y.** (2004). A new method for rapid visualization of defects in leaf cuticle reveals five intrinsic patterns of surface defects in *Arabidopsis.* Plant J. **37:** 139–146.

**Tang, W., Kelley, D., Ezcurra, I., Cotter, R., and McCormick, S.** (2004). LeSTIG1, an extracellular binding partner for the pollen receptor kinases LePRK1 and LePRK2, promotes pollen tube growth *in vitro.* Plant J. **39:** 343–353.

**Tierney, M.L., and Varner, J.E.** (1987). The extensins. Plant Physiol. **84:** 1–2.

**Tsuwamoto, R., Fukuoka, H., and Takahata, Y.** (2008). GASSHO1 and GASSHO2 encoding a putative leucine-rich repeat transmembrane-type receptor kinase are essential for the normal development of the epidermal surface in Arabidopsis embryos. Plant J. **54:** 30–42.

**Verhoeven, T., Feron, R., Wolters-Arts, M., Edqvist, J., Gerats, T., Derksen, J., and Mariani, C.** (2005). STIG1 controls exudate secretion in the pistil of petunia and tobacco. Plant Physiol. **138:** 153–160.

**Winter, D., Vinegar, B., Nahal, H., Ammar, R., Wilson, G.V., and Provart, N.J.** (2007). An "Electronic Fluorescent Pictograph" browser for exploring and analyzing large-scale biological data sets. PLoS One **2:** e718.

**Wrzaczek, M., et al.** (2015). GRIM REAPER peptide binds to receptor kinase PRK5 to trigger cell death in Arabidopsis. EMBO J. **34:** 55–66.

**Xing, Q., Creff, A., Waters, A., Tanaka, H., Goodrich, J., and Ingram, G.C.** (2013). ZHOUPI controls embryonic cuticle formation via a signalling pathway involving the subtilisin protease ABNORMAL LEAF-SHAPE1 and the receptor kinases GASSHO1 and GASSHO2. Development **140:** 770–779.

**Yang, S., Johnston, N., Talideh, E., Mitchell, S., Jeffree, C., Goodrich, J., and Ingram, G.** (2008). The endosperm-specific ZHOUPI gene of *Arabidopsis thaliana* regulates endosperm breakdown and embryonic epidermal development. Development **135:** 3501–3509.